Extraordinary optical absorption based on guided-mode resonance

Wenchao Zhou,[1,2] Yihui Wu,[1,*] Muxin Yu,[1,2] Peng Hao,[1] Guigen Liu,[1] and Kaiwei Li[1,2]

[1]*State Key Laboratory of Applied Optics, Changchun Institute of Optics, Fine Mechanics and Physics, Chinese Academy of Sciences, 3888 Dongnanhu Road, Changchun 130033, China*

[2]*University of Chinese Academy of Sciences, Beijing 100039, China*

**Corresponding author: yihuiwu@ciomp.ac.cn*

Received August 13, 2013; revised October 29, 2013; accepted November 13, 2013; posted November 13, 2013 (Doc. ID 195581); published December 10, 2013

We propose a novel structure that can achieve extraordinary optical absorption over the visible spectrum, based on the guided-mode resonance effect. An optical metal grating with moderate thickness and high filling factor can lead to coupling between the quasi-guided-mode and cavity mode. The resonant interaction between the two modes can influence the field distribution, such as the magnetic field near the grating, which results in extraordinary absorption. Absorption efficiency can be optimized up to 99.16%. We also show that the absorption peak can be readily tuned just by varying the subwavelength grating period. © 2013 Optical Society of America

OCIS codes: (050.0050) Diffraction and gratings; (240.6680) Surface plasmons; (260.5740) Resonance; (310.6628) Subwavelength structures, nanostructures; (350.2450) Filters, absorption.

http://dx.doi.org/10.1364/OL.38.005393

In recent years, extraordinary optical absorption in nanostructures has attracted much attention because of its potential application in photodetectors and photovoltaics [1–4]. A tremendous number of structures have been proposed, such as plasmonic nanostructures [5–7] and metamaterial absorbers [8–14]. Among these structures, metamaterial absorbers have attracted considerable interest due to their unique electromagnetic properties, such as the feasibility of arbitrary effective permittivity and permeability originating from the electromagnetic resonance inside the metamaterial structures [11]. However, to achieve nearly perfect absorption, a perfect impedance, matching the surrounding environment, must be satisfied. Simultaneously, the imaginary parts of effective permittivity and permeability should be manipulated to high dissipation factors inside the metamaterials, considering the energy loss proportional to these two parameters [15]. In addition, the impedance at resonance should depend on the dimensions of the structures and the physical properties of the materials. Perfect impedance matching needs tighter fabrication tolerances to obtain an absorption peak that is very sensitive to geometrical adjustment [11]. These factors make the absorber design more complicated. Recently, the coupling between surface plasmon polariton (SPP) modes and the cavity modes (CMs) was investigated and found to enhance absorption efficiency up to 75% [16]. However, the resulting efficiency is relatively low because of the downward transmission through the metal slit and the upward reflection of the metal ridge. In this Letter, we propose a novel structure to obtain nearly perfect absorption (>90%), based on the guided-mode resonance (GMR) effect. The GMR effect can be exploited to design reflection filters [17] or transmission filters [18,19] by virtue of their simple structures and nearly 100% diffraction efficiency for a given operating wavelength. However, to our knowledge, few studies have focused on the absorption feature with the GMR effect. In our structure, we substitute the metal mirror in the metal–insulator–metal (MIM) metamaterial structure investigated in previous works [15] with a waveguide layer that can be used to support the quasi-guided mode (QGM). Though the coupling between the waveguide mode and plasmonic mode has been investigated in hybrid waveguide configurations to achieve subwavelength mode confinement and low propagation loss [20–23], in this Letter, the coupling between the QGM and the CM gives rise to extraordinary optical absorption.

Figures 1(a) and 1(b) show the proposed structure, comprising a two-dimensional aluminum grating with a high filling factor and a waveguide structure. The waveguide structure can be formed by the $SiO_2/Si_3N_4/Quartz$ (SiO_2). The structure is illuminated from the top by a plane wave, with its magnetic field polarized normal to the incident plane (y direction). A numerical analysis of the electromagnetic field features was performed by utilizing rigorous coupled wave analysis (RCWA) [24,25]. In all numerical simulations, we estimated the

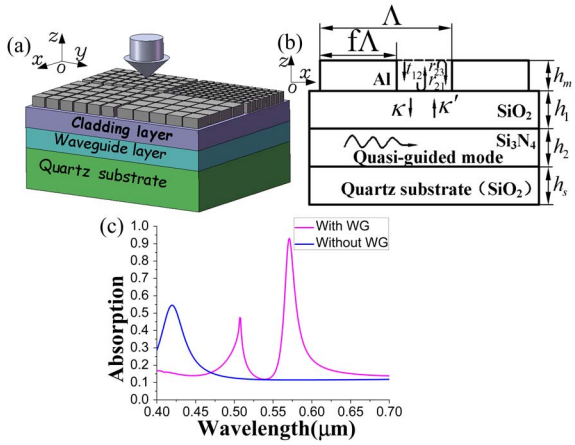

Fig. 1. (a) Schematic diagram of the proposed two-dimensional metal subwavelength grating. (b) Front view showing the structural parameters and the relevant scattering and coupling coefficients. (c) Absorption spectra with and without the waveguide (WG) structure.

complex optical dielectric function of the metal grating using the Lorentz–Drude model, taking into account interband transitions [26]. Meanwhile, we fixed the refraction indices of SiO_2 and Si_3N_4 as 1.45 and 2.0, respectively. To attain the resonant peak, we solve the eigenmode equation of the waveguide structure below the metal grating. The propagation constant of the guided mode can be provided by the first-order grating diffraction of incident light [19]. Both the cladding thickness and waveguide layer are 0.1 μm. As shown in Fig. 1(c), an extraordinary optical absorption peak can be obtained in the proposed structure with the waveguide underneath the aluminum grating, compared with a freestanding grating. Therefore, the waveguide structure is essential to obtain >90% absorption efficiency. We argue that the enhanced absorption originates from the coupling between the QGM, which resulted from diffraction of the incident light [19], and the CM, supported inside the slits, which acts as a truncated MIM plasmon waveguide, as shown in Fig. 1(b). Truncation of such a waveguide results in strong reflections at the slit terminations, and a resonant cavity can subsequently form. With the introduction of the metal grating, the plane wave can couple to SPPs on the air/aluminum, or SiO_2/aluminum interface, at a specific resonant wavelength, when the wave vector of the SPP mode matches the diffracted light. Meanwhile, a resonant coupling is possible between the incident light and the guided mode of the planar waveguide, which can be considered a metal grating GMR [18]. This coupled guided mode in the waveguide layer becomes a quasi-guided (leaky) mode because of the periodic modulation of the metal grating. The scattered waves will radiate into the far-field in the forward direction, without any coupling. Furthermore, in the resonant cavity, the incident light can also excite the CM, which has a behavior similar to the gap plasmon mode supported by the slit, with a transmission coefficient t_{12}. As depicted in Fig. 1(b), at the top and bottom interfaces, the propagating plasmon experiences multiple reflections, with complex reflection coefficients r_{12} and r_{23}, respectively, and which include a magnitude and phase. We assumed that the QGM could couple with the CM, with the coupling coefficient κ at a certain frequency. The eigenfrequencies of the CM resonance are determined by the resonant length h_m, and given by the formula [27]:

$$\phi_{12} + \phi_{23} + k_{MIM} h_m = 2m\pi, \tag{1}$$

where ϕ_{12} and ϕ_{23} are phases acquired by the CM and caused by the reflection at the two terminations, m is the resonance order integer, and k_{MIM} is the complex wave vector of the plasmon mode in the slits [28].

Initially, we speculate, some of the incident light excites the QGM directly through the resonant tunneling effect and that the other light simultaneously excites the CM around the coupling point. In addition, the coupling between QGM and CM then occurs through the evanescent field. To clarify the coupling point, we have calculated the transmission and absorption spectrum dependence on grating thickness, with a grating period of 0.35 μm, as represented in Figs. 2(a) and 2(b). We observe that the transmission peaks coincide with the

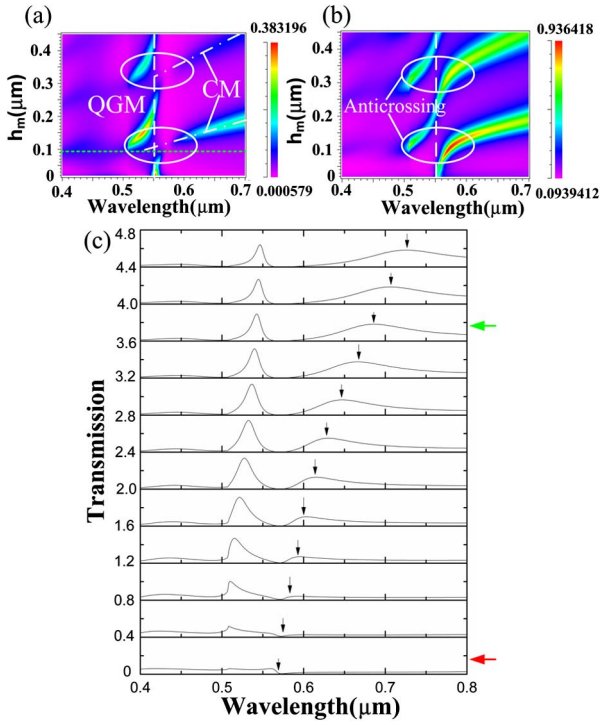

Fig. 2. (a) and (b) Transmission and absorption spectra, respectively, plotted as a function of incident wavelength and grating thickness (h_m), period $\Lambda = 0.35$ μm, and filling factor $f = 0.9$. The elliptical circle denotes the anticrossing coupling. Calculated QGM and the CM are marked with a dashed line and dash–dot line, respectively. Under the green (small) dot, the grating cannot support CM. (c) Transmission spectra with grating thickness ranging from 0.09 to 0.2 μm (down to top), in steps of 0.01 μm. The black arrow indicates the CM. On the right side of the picture, the green and red arrows show the grating thicknesses 0.09 and 0.18 μm, respectively.

absorption peaks; hence, it indicates that both the enhanced transmission and the extraordinary absorption can be attributed to the same resonant excitation of a certain mode in the structure. If the metal grating is thick enough to support CMs, then SPPs can also be excited at the same time, under the wave vector matching condition. These two modes can be considered as the cause of extraordinary optical transmission (EOT) in most previous works [29]. Besides these modes, QGM that is related to the waveguide structure is another mechanism for enhanced transmission [19]. In the present study, the QGM and the CM are the main factors in the EOT effect.

In general, different modes cannot interact with one another. However, if we decrease the metal thickness gradually, the coupling between CM and QGM becomes increasingly significant. Under the moderate grating thickness, the QGM can couple effectively with the CM, instead of transmitting through the periodic modulation. This mode coupling causes an anticrossing of the resonance, observed in the simulated transmission and absorption spectra. Figure 2(c) displays the transmission spectra with grating thickness ranging from 0.09 to 0.2 μm in steps of 0.01 μm. Apparently, as the thickness of the metal grating decreases, the transmission peak caused by the QGM coupling is kept nearly constant.

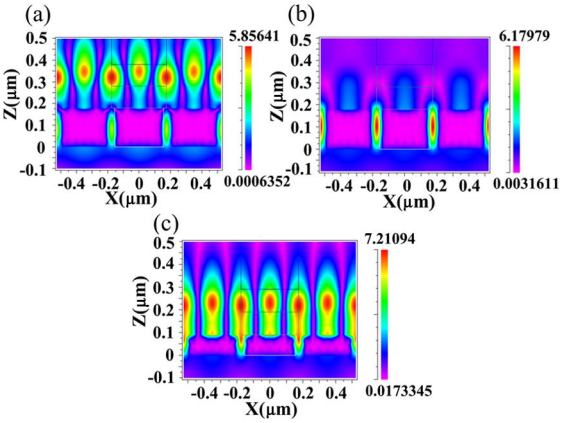

Fig. 3. (a) and (b) Magnetic field component Hy for the grating thickness $h_m = 0.18$ μm, denoted by the green arrow, as shown in Fig. 2(c). (a) SPP mode ($\lambda = 0.543$ μm), (b) CM ($\lambda = 0.686$ μm), and (c) The magnetic field for the grating thickness $h_m = 0.09$ μm at the anticrossing coupling point ($\lambda = 0.567$ μm). The solid lines in these figures show the grating configuration. Metal grating, cladding layer, waveguide layer, and substrate are depicted from bottom to top, respectively.

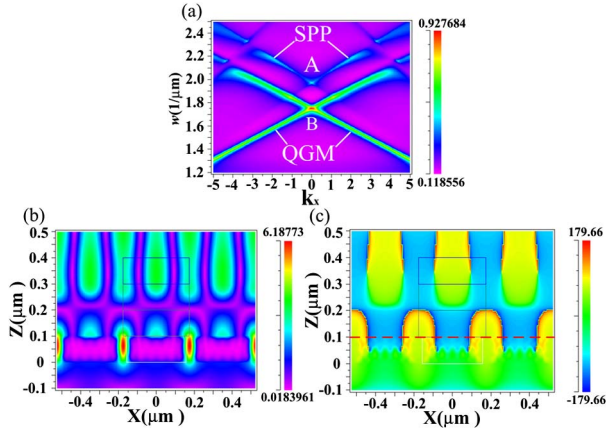

Fig. 5. (a) Absorption spectrum dependence on the incident frequency and the in-plane wave vector. (b) and (c) The amplitude and the phase distribution at point A, respectively. In (a), the white arrows denote the SPP mode and the QGM mode, which can cause the absorption. The red dash indicates the interface between the metal grating and the cladding layer.

However, the CM peak blueshifts until coupling with the QGM mode. Meanwhile, we note that the transmission efficiency becomes smaller, step by step. In contrast, the absorbance increases gradually, as shown in Fig. 2(b). Therefore, more energy is absorbed at the coupling region.

To gain further insight into the physical origin of the absorption peak, the numerically calculated magnetic field Hy, with grating thicknesses of 0.18 and 0.09 μm, is shown in Fig. 3. Under the grating thickness $h_m = 0.18$ μm, there are two transmission peaks, displayed by the green arrow in Fig. 2(c). As mentioned above, these peaks result from the QGM and CM presented in Figs. 3(a) and 3(b). However, at the anticrossing coupling region, such as when the grating thickness $h_m = 0.09$ μm, the presence of the QGM modifies the optical response of the structure in the CM vicinity, as shown in Fig. 3(c). This modification reinforces the energy around the grating boundary, which causes the extraordinary optical absorption.

The coupling between the QGM and the CM results in a pronounced absorption. Since the QGM is proportional to the grating period, so the absorption peak can be adjusted readily via the period depicted in Fig. 4. As expected, the resonant length should increase with the redshift of the resonant wavelength in CM. However, we can get distinct absorption peaks with the different grating periods while keeping the resonant length constant (as displayed in Fig. 4), although k_{MIM} decreases as the slit width $[(1-f)\,P)]$ increases, because of the grating period increment. The phase pickup ϕ on the reflection increases as the slit width increases with a contrary trend, resulting in a nearly constant resonant length [28,30]. We can also observe another absorption peak that is displayed in the elliptical circle near the dominant absorption peak induced by the coupled mode of QGM and CM. To explain this phenomenon, we investigated the absorption dispersion diagram of the structure in Fig. 5. The variable $w = 1/\lambda$ stands for the frequency and $k_x = 2\pi\,\sin(\theta)/\lambda$ represents the x component of the incident wave vector. Based on Fig. 5, we can conclude that the sub-peak is ascribed to another SPP mode, as displayed in Fig. 5(a). The magnetic field is found to be confined at the interface of Al/SiO_2, demonstrating the clear SPP characteristics, as shown in Figs. 5(b) and 5(c). The coupling between SPP and CM causes the absorption enhancement [16]. From Fig. 5(a), we can also note that the absorption efficiency for oblique incidence is less than that of the main coupling at $k_x = 0$, such that the optimal coupling point occurs under the normal incidence. That is, the absorption maximum appears when the incident angle equals 0.

In addition to the parameters mentioned above, high filling factor f is indispensable to acquire the great absorption efficiency demonstrated in Fig. 6. From this figure, no apparent change is observed on the resonant wavelength over a fill factor range of 0.8–0.95. Thus, this

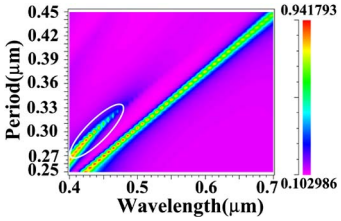

Fig. 4. Absorption spectrum dependence on the grating period with constant 0.10 μm grating thickness.

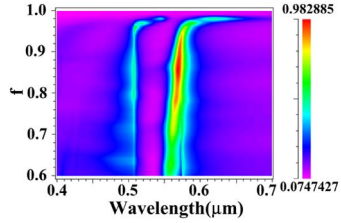

Fig. 6. Absorption spectrum plotted as a function of the filling factor ($h_m = 0.10$ μm, period = 0.35 μm).

absorption structure has good fabrication tolerances against the fill factor.

In the content above, we only calculated the absorption efficiency numerically, with some fixed structure parameters, such as thickness and filling factor. The maximum absorption efficiency can be as high as 99.16% at 0.593 μm wavelength, with 0.107 μm grating thickness, 0.854 filling factor, 0.094 μm cladding thickness, and 0.0719 μm waveguide layer thickness. The optimization principle is based on the simplex algorithm [31].

In conclusion, high absorption (maximum value 99.16%) on the basis of a GMR with two-dimensional aluminum grating, can be obtained under normal incidence because of the coupling between the QGM and the CM. We study the gradual coupling process by changing the metal grating thickness and demonstrate the magnetic field distribution to gain a clear insight. We can obtain distinct absorption peaks in the visible region by varying the grating period. This type of absorber has good fabrication tolerances against the fill factor. Thus, the extraordinary optical absorption could be exploited in numerous photonic applications, such as photodetectors, biosensors, and so on.

This work is supported by the National High Technology Research and Development Program (No. 2012AA040503), National Key Foundation (No. 11034007), and National Science for Youth Foundation (No. 61102023) of China. Wenchao Zhou also acknowledges the fruitful discussions with Associate Prof. Chunyin Qiu from Wuhan University and Prof. Ruey-Lin Chern from National Taiwan University.

References

1. Z. Yu, G. Veronis, S. Fan, and M. L. Brongersma, Appl. Phys. Lett. **89**, 151116 (2006).
2. J. Rosenberg, R. V. Shenoi, T. E. Vandervelde, S. Krishna, and O. Painter, Appl. Phys. Lett. **95**, 161101 (2009).
3. J. J. Talghader, A. S. Gawarikar, and R. P. Shea, Light Sci. Appl. **1**, e24 (2012).
4. R. A. Pala, J. White, E. Barnard, J. Liu, and M. L. Brongersma, Adv. Mater. **21**, 3504 (2009).
5. P. Zhu and L. J. Guo, Appl. Phys. Lett. **101**, 241116 (2012).
6. J. N. Munday and H. A. Atwater, Nano Lett. **11**, 2195 (2011).
7. L. Meng, D. Zhao, Q. Li, and M. Qiu, Opt. Express **21**, A111 (2013).
8. N. Liu, M. Mesch, T. Weiss, M. Hentschel, and H. Giessen, Nano Lett. **10**, 2342 (2010).
9. Y. Wang, T. Sun, T. Paudel, Y. Zhang, Z. Ren, and K. Kempa, Nano Lett. **12**, 440 (2012).
10. B. Zhang, J. Hendrickson, and J. Guo, J. Opt. Soc. Am. B **30**, 656 (2013).
11. N. I. Landy, S. Sajuyigbe, J. J. Mock, D. R. Smith, and W. J. Padilla, Phys. Rev. Lett. **100**, 207402 (2008).
12. Y. Cui, K. H. Fung, J. Xu, H. Ma, Y. Jin, S. He, and N. X. Fang, Nano Lett. **12**, 1443 (2012).
13. M. Diem, T. Koschny, and C. M. Soukoulis, Phys. Rev. B **79**, 033101 (2009).
14. R. Alaee, M. Farhat, C. Rockstuhl, and F. Lederer, Opt. Express **20**, 28017 (2012).
15. J. Hao, L. Zhou, and M. Qiu, Phys. Rev. B **83**, 165107 (2011).
16. A. Roszkiewicz and W. Nasalski, Opt. Lett. **37**, 3759 (2012).
17. Z. S. Liu, S. Tibuleac, D. Shin, P. P. Young, and R. Magnusson, Opt. Lett. **23**, 1556 (1998).
18. E. Sakat, G. Vincent, P. Ghenuche, N. Bardou, S. Collin, F. Pardo, J. L. Pelouard, and R. Haidar, Opt. Lett. **36**, 3054 (2011).
19. A. F. Kaplan, T. Xu, and L. J. Guo, Appl. Phys. Lett. **99**, 143111 (2011).
20. R. F. Oulton, V. J. Sorger, D. A. Genov, D. F. P. Pile, and X. Zhang, Nat. Photonics **2**, 496 (2008).
21. D. Dai and S. He, Opt. Express **17**, 16646 (2009).
22. Y. Bian, Z. Zheng, X. Zhao, J. Zhu, and T. Zhou, Opt. Express **17**, 21320 (2009).
23. Y. Bian, Z. Zheng, X. Zhao, Y. Su, L. Liu, J. Liu, J. Zhu, and T. Zhou, IEEE J. Sel. Top. Quantum Electron. **19**, 4800106 (2013).
24. M. G. Moharam and T. K. Gaylord, J. Opt. Soc. Am. A **3**, 1780 (1986).
25. S. Peng and G. M. Morris, J. Opt. Soc. Am. A **12**, 1087 (1995).
26. A. D. Rakic, A. B. Djurisic, J. M. Elazar, and M. L. Majewski, Appl. Opt. **37**, 5271 (1998).
27. J. S. White, G. Veronis, Z. Yu, E. S. Barnard, A. Chandran, S. Fan, and M. L. Brongersma, Opt. Lett. **34**, 686 (2009).
28. J. A. Dionne, L. A. Sweatlock, and H. A. Atwater, Phys. Rev. B **73**, 035407 (2006).
29. F. J. Garcia-Vidal, L. Martin-Moreno, T. W. Ebbesen, and L. Kuipers, Rev. Mod. Phys. **82**, 729 (2010).
30. R. Gordon, Phys. Rev. B **73**, 153405 (2006).
31. W. H. Press, S. A. Teukolsky, W. T. Vetterling, and B. P. Flannery, *Numerical Recipes in C*, 2nd ed. (Cambridge University, 1995), pp. 394–444.